Pergamon

Int. J. Heat Mass Transfer. Vol. 39, No. 14, pp. 2869–2882, 1996

0017-9310/96 $15.00+0.00

0017-9310(95)00378-9

Numerical study on mode-transition of natural convection in differentially heated inclined enclosures

C. Y. SOONG and P. Y. TZENG

Department of Aeronautical Engineering, Chung Cheng Institute of Technology, Taoyuan, Taiwan 33509, Republic of China

and

D. C. CHIANG and T. S. SHEU

Department of System Engineering, Chung Cheng Institute of Technology, Taoyuan, Taiwan 33509, Republic of China

(*Received* 6 *March* 1995 *and in final form* 6 *November* 1995)

Abstract—The present paper reports a numerical investigation of natural convection and the associated mode-transition and hysteresis phenomena in a two-dimensional differentially heated inclined enclosure. Unsteady Navier–Stokes/Boussinesq equations governing the fluid flow and heat transfer are solved numerically. Rayleigh numbers in steady flow regime, $1 \times 10^3 \leqslant Ra \leqslant 2 \times 10^4$, and the angles of inclination of $0° \leqslant \gamma \leqslant 90°$ are considered in the computations. Major concerns are the effects of inclination on flow-mode transition. Enclosures of length-to-height aspect ratio $As = 4$, 3 and 1 are studied. Air of $Pr = 0.71$ in an enclosure of $As = 4$ is chosen as the flow model to examine the influences of the inclination at various Rayleigh numbers. Hysteresis phenomena for $Ra \geqslant 2000$ are demonstrated. Parameter maps of Ra vs γ for $As = 4$ with γ increasing and decreasing are proposed, in which flow regimes characterized by various modes are designated. Effects of initial condition on the flow pattern formation are examined for $As = 3$. In a model of square enclosure ($As = 1$), effect of the imperfect thermal boundary conditions is examined to investigate the possible causes for inconsistency of the predictions with the experiments. The present study provides more physical insight into the natural convection in enclosures. Copyright © 1996 Elsevier Science Ltd.

INTRODUCTION

Thermally driven flow and heat transfer in fluid layers and enclosures have attracted considerable attention due to their relevance to a variety of engineering applications such as solar energy collectors, crystal growth reactors, multilayered walls and double windows, etc. On the other hand, this class of flows can be employed as a theoretical model for investigation of some fundamental hydrodynamic natures such as thermal instability, bifurcation and chaotic behaviors of the nonlinear flow systems. These issues are significant and closely related to the exploration of transition to turbulence. In inclined enclosures, orientation of the flow system changes the buoyancy force components and the resultant flow structure. The issues mentioned above have been discussed in the review article by Yang [1]. In the past decades, tremendous amount of papers on this field have appeared. Instead of an exhaustive literature survey, only those closely related to the present study, i.e. two-dimensional steady-flow regime, are addressed herein. A detailed review of natural convection in enclosures can be found elsewhere.

Probably, the experimental work by Dropkin and Somerscales [2] was the first study on inclined enclosure in a heat transfer viewpoint. The pioneering stability analysis with a companion experiment was performed by Hart [3]. Through heat transfer measurements, Hollands and Konicek [4] confirmed a change-over angle, at which it was presumably caused by a transition between two different flow patterns. In a later work, Arnold *et al.* [5] also demonstrated the existence of this change-over phenomenon.

Catton *et al.* [6], by using Galerkin method, solved two-dimensional flow and temperature fields in inclined enclosures of various aspect ratios. In a more recent numerical study [7] with stress on heat transfer rates, a penalty function finite element method was employed to solve the problem of natural convection in inclined enclosure. In the above-mentioned numerical works, however, only limited information about flow patterns was provided.

The studies, either numerical and experimental, by Ozoe and his colleagues [8–13] are quite noteworthy. In an experiment [8] of glycerol in a square enclosure (in two-dimensional sense), they found a mismatch in

NOMENCLATURE

As	aspect ratio, L/H
g	gravitational acceleration [m s^{-2}]
H	height of the side walls [m]
L	length of the heating wall [m]
Nu	mean Nusselt number
P,P'	dimensional pressure and pressure departure from the reference state [N m^{-2}]
p,p'	dimensionless pressure and pressure departure, $p' = p - p_r = P'/\rho U^2$
Pr	Prandtl number, ν/α
Ra	Rayleigh number, $g\beta(T_h - T_c)H^3/\alpha\nu$
t	time [s]
T	temperature [K]
U, V	dimensional velocity components [m s^{-1}]
u, v	dimensionless velocity components
X, Y	Cartesian coordinates [m]
x, y	dimensionless coordinates.

Greek symbols

α	thermal diffusivity [m^2 s^{-1}]
β	thermal expansion coefficient [K^{-1}], $-(\partial\rho/\partial T)_p/\rho$
γ	inclination angle [deg]
ε	perturbation parameter
ψ	dimensionless stream function
θ	dimensionless temperature function, $(T - T_c)/(T_h - T_c)$
ρ	density [kg m^{-3}]
τ	dimensionless time, $t\alpha/H^2$
ν	kinematic viscosity [m^2 s^{-1}].

Subscripts

c	cold wall; critical
h	hot wall
i	initial
max	maximum
min	minimum
r	reference.

heat transfer rates between measured data and the two-dimensional calculations. Later on, Ozoe *et al.* [13] claimed that the inconsistency was attributed to the three-dimensional effect in experiments. To examine the flow structure in the inclined enclosures, Ozoe *et al.* [9, 10, 12] also conducted some flow visualization studies by using aluminum powder as tracer. For reduction of the computational efforts, Ozoe *et al.* [11, 12] calculated the flow at $Ra = 4000$ in a $2 \times 2 \times 1$ box for comparison with the observations at $Ra = 12\,000$. By using the same strategy with changes in boundary conditions at the side boundaries, e.g. free–free or free–rigid, Ozoe *et al.* [14] also simulated the influence of the rigid wall on the streakline patterns in inclined cells.

In the review presented above, it implies that the transition of the flow-modes or flow patterns may occur as inclination angle or Rayleigh number changes, and the heat transfer rates may be drastically altered by the mode-transition. As that mentioned by Ozoe *et al.* [8], in some situations, numerical calculation can not catch the same trend of inclination effect on heat transfer rates as that obtained in experiments. In the present authors' viewpoint, difficulties in control of isothermal wall condition may be a major reason for the inconsistency. In fact, this class of natural convection, especially that at zero or small inclination angles, is very sensitive to the initial and boundary conditions. In a recent numerical study on oscillatory natural convection, Okada and Ozoe [15] demonstrated the significant effects of initial condition on the computational results. Sparrow *et al.* [16] have investigated the effect of boundary conditions, isothermal or iso-flux, on the onset of thermal instability in a horizontal fluid layer. In a recent work of Kessler [17], thermal boundary conditions of conducting as well as adiabatic side walls were considered. Their studies disclosed that different flow patterns can be constructed for different thermal boundary conditions. In a most recent study, Gau and Jeng [18], by using an electrochemical method, conducted an experiment with companion numerical computations for transient natural convection in inclined enclosures. No inconsistency mentioned above was found in their study since they did not need to maintain uniformity of the wall temperatures in the experiments. It is believed that the imperfection of the isothermal wall conditions in experiments is a crucial factor and is worthy of investigation.

In the present work, two-dimensional computations are performed for natural convection and the associated mode transition phenomena in a two-dimensional differentially heated inclined enclosure. Navier–Stokes/Boussinesq equations governing the fluid flow and heat transfer are solved by a finite-volume method. The Rayleigh numbers in steady flow regime, $1 \times 10^3 \leqslant Ra \leqslant 2 \times 10^4$, and the angles of inclination of $0 \leqslant \gamma \leqslant 90°$ are considered in the computations. To check the present numerical procedure, the calculated thermally driven flow solutions in a square cavity are compared with the benchmark solutions [19]. Major concerns are the effects of inclination on the flow-mode transition, which can in turn alter the heat transfer rates of the system. Enclosures of $As = 1$, 3 and 4 are considered. Air of $Pr = 0.71$ in an enclosure of aspect-ratio $As = 4$ is chosen as the flow model to examine the influences of the inclination at various Rayleigh numbers. Hysteresis phenomenon occurring

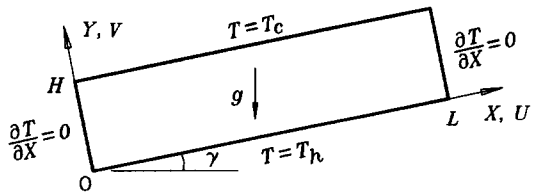

Fig. 1. Physical model of the inclined enclosure.

in the courses of increasing and decreasing inclination is also studied. Parameter maps of Ra vs γ for $As = 4$ with increasing as well as decreasing inclination are proposed, in which flow regimes characterized by various modes are designated. Influences of the initial condition on the flow pattern formation are also examined for an enclosure of $As = 3$. By considering silicon oil in a square enclosure ($As = 1$) studied in the work of Ozoe *et al.* [8], effect of the imperfect thermal boundary condition on flow solutions is investigated to explore the possible causes for inconsistency of the predictions and the experiments.

PROBLEM STATEMENT

Consider a two-dimensional inclined rectangular enclosure of length L and height H as shown in Fig. 1. The two side walls are insulated, and the fluid is heated and cooled at the other two opposite walls, respectively. The fluid is assumed to be of constant properties and the Boussinesq approximation is employed for the gravity terms. Stress–work are neglected. In the present study, H, H^2/α and α/H are used, respectively, as the length, time and velocity scales, where α denotes the thermal diffusivity. The dimensionless temperature function is defined as $\theta = (T - T_r)/\Delta T$, in which $\Delta T = T_h - T_c$ stands for the temperature difference of the two isothermal walls and $T_r = T_c$ is the fluid temperature at reference state. The governing equations in dimensionless form can be cast into the following form,

$$\partial u/\partial x + \partial v/\partial y = 0 \tag{1}$$

$$\partial u/\partial \tau + u\,\partial u/\partial x + v\,\partial u/\partial y = Pr\nabla^2 u - \partial p'/\partial x + RaPr\sin\gamma\theta \tag{2}$$

$$\partial v/\partial \tau + u\,\partial v/\partial x + v\,\partial v/\partial y = Pr\nabla^2 v - \partial p'/\partial y + RaPr\cos\gamma\theta \tag{3}$$

$$\partial\theta/\partial\tau + u\,\partial\theta/\partial x + v\,\partial\theta/\partial y = \nabla^2\theta \tag{4}$$

where $p' = p - p_r$ is pressure departure from the reference pressure p_r, $Ra = \beta g(T_h - T_c)H^3/\alpha\nu$ is the Rayleigh number, $Pr = \nu/\alpha$ is the Prandtl number, β is the thermal expansion coefficient and ν is the kinematic viscosity. No-slip condition is imposed at four walls of the enclosure. Two side walls are thermally insulated, whereas the other two opposite walls are kept at the uniform temperatures T_h and T_c, respectively. The boundary conditions for the system of equations (1)–(4) are

$$u = v = 0 \quad \text{at four walls}$$

$$\partial\theta/\partial x = 0 \quad \text{at} \quad x = 0 \quad \text{and} \quad x = As$$

$$\theta = 1 \quad \text{at} \quad y = 0 \quad \text{and} \quad \theta = 0 \quad \text{at} \quad y = 1$$

where As is the length-to-height aspect ratio of the enclosure.

NUMERICAL PROCEDURE

The system of equations (1)–(4) with the boundary conditions stated above is solved by using finite volume method and the SIMPLE-C algorithm [20]. Since

Table 1. Comparison of the thermally-driven cavity flow solution

Quantities	Benchmark [19]	Present	Deviation
	$Ra = 10^3$		
u_{max}	3.649(x,y) = (0.5,0.813)	3.632(x,y) = (0.5,0.818)	−0.5%
v_{max}	3.697(x,y) = (0.181,0.5)	3.697(x,y) = (0.178,0.5)	0.0%
Nu	1.118	1.120	0.2%
Nu_{max}	1.505	1.514	0.6%
Nu_{min}	0.692	0.688	−0.6%
	$Ra = 10^4$		
u_{max}	16.178(x,y) = (0.5,0.823)	16.194(x,y) = (0.5,0.819)	0.1%
v_{max}	19.617(x,y) = (0.119,0.5)	19.656(x,y) = (0.123,0.5)	0.2%
Nu	2.243	2.246	0.1%
Nu_{max}	3.528	3.534	0.2%
Nu_{min}	0.586	0.587	0.2%
	$Ra = 10^5$		
u_{max}	34.73(x,y) = (0.5,0.855)	35.43(x,y) = (0.5,0.863)	2.0%
v_{max}	68.59(x,y) = (0.066,0.5)	68.60(x,y) = (0.068,0.5)	0.0%
Nu	4.519	4.511	−0.2%
Nu_{max}	7.717	7.691	−0.3%
Nu_{min}	0.729	0.736	1.0%

Table 2. Grid-dependence of natural convection solutions at $Ra = 10^4$ and $Pr = 0.71$ in a horizontal enclosure of $As = 4$

Grid	$\frac{Nu_h}{Nu_c}$	(% Dev.)	$\frac{Nu_h}{Nu_c}$	u_{max}	(% Dev.)	v_{max}	(% Dev.)
121×31	2.50326	(−0.76)	2.1×10^{-4}	27.54072	(−2.10)	30.65512	(−2.87)
	2.50347	(−0.75)					
161×41	2.51604	(−0.25)	1.3×10^{-4}	27.97881	(−0.59)	31.23646	(−1.03)
	2.51617	(−0.25)					
201×51	2.52234	(—)	9.0×10^{-5}	28.14584	(—)	31.56145	(—)
	2.52243	(—)					

the flow fields for the parameter range considered lie in the steady flow regime, the time marching nature of the computation is simply a pseudo-transient technique. The value of $\Delta\tau = 10^{-3}$ is used through the course of the computation. A non-uniform staggered grid with the grid lines clustered toward the walls is employed. As the maximum relative deviation of the mean Nusselt numbers between two successive time-steps is less than the value of 10^{-4} or the maximum value of the relative deviation of the velocity u less than 10^{-5}, the procedure is regarded as converged.

To check the validity of the present numerical procedure, thermally driven flows in a square cavity were solved. The present predictions and the corresponding benchmark solutions [19] are listed in Table 1. For Ra up to 10^5, the comparison shows quite good agreement in either maximum velocities and mean Nusselt numbers. Also, a grid experiment was performed before the course of the computations. A typical case with $As = 4$, $Ra = 10\,000$, $\gamma = 0°$ and $Pr = 0.71$ was calculated on the grids of 121×31, 161×41 and 201×51. The test results of mean Nusselt numbers, and the maximum velocities u_{max} and v_{max} are listed in Table 2. Based on the finest grid (201×51) solutions, the deviations of the results on the relatively coarser grids are shown in the parentheses. The solutions on a grid of 161×41 are very close to the ones on the finest grid, and the differences between the hot-wall and the cold-wall Nusselt numbers, $Nu_h - Nu_c$, are small enough. It is believed that the grid of 161×41 points is appropriate in the present computations.

Since the problem is very sensitive to the initial guess or initial condition (in the pseudo-unsteady sense) and the hysteresis phenomenon is one of the major concerns in the study, the sequence of the

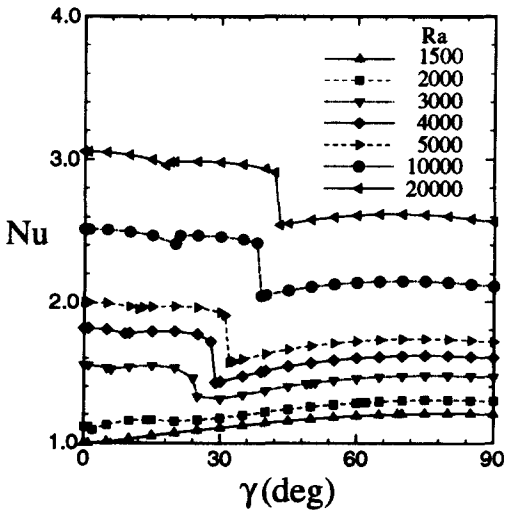

Fig. 2. Average Nusselt numbers at various γ and Ra (γ-increasing).

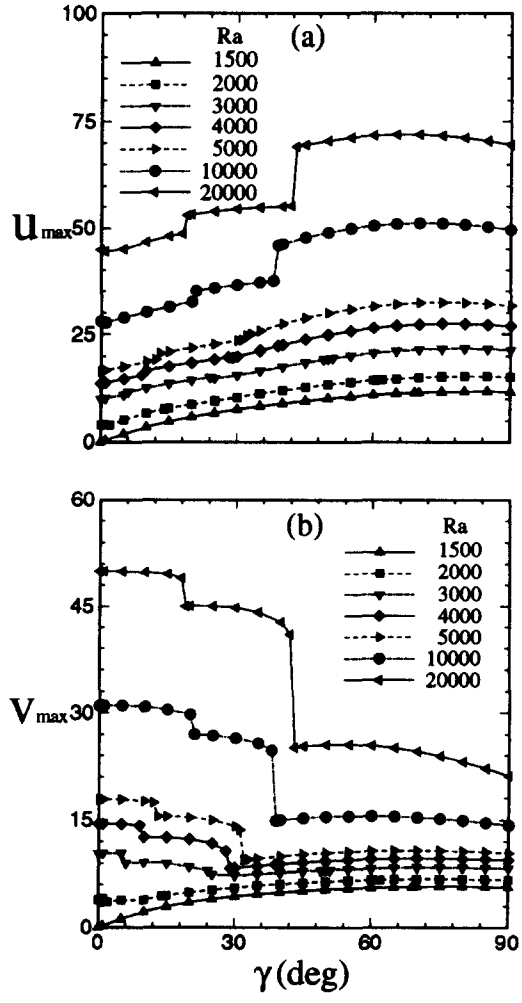

Fig. 3. Maximum velocities at various γ and Ra (γ-increasing), (a) u_{max}, (b) v_{max}.

numerical solution should be specified clearly. In computations with γ increasing from 0° to 90°, flow and temperature fields at a fixed value of Ra in horizontal enclosure ($\gamma = 0°$) are first solved. For $\gamma = 0°$, the initial guess of the velocity field is null and the initial temperature field is $\theta_i \equiv 0$. The zero-inclination solution is employed as the initial condition for solution of the subsequent case of inclination, say $\gamma = 5°$. The latter solution is then used to initiate the computation of the flow solution at, say, $\gamma = 10°$, and so on. As the γ-range in which mode-transition occurs, say γ between 25° and 30°, a smaller increment of $\Delta\gamma = 1°$ is employed to locate mode-transition angle within 1° accuracy. After the solutions at $\gamma = 90°$ are obtained, it is used as the initial guess for solution of a lower inclination. Then the similar procedure proceeds continuously back to $\gamma = 0°$.

The computations in the present work were performed on an HP-750 workstation. Only one iteration is performed in a time-step. In general, the number of the pseudo-time steps needed for convergent or steady-state solution is of the order of 10^4. It took about 0.25 s for a single time-step. For Rayleigh numbers near the critical point, e.g. $Ra = 1500$ and 2000, the convergence rate is very slow and the computational time is almost one order longer than a general case.

RESULTS AND DISCUSSION

Heat transfer rates in the course of γ increasing

Figure 2 displays the mean heat transfer rates, Nu, at various Rayleigh numbers and inclination angles. Since, for zero-inclination, the critical Rayleigh number is about 1800, Nu is still kept as 1.0 for $Ra = 1500$. As the enclosure is tilted, the upward buoyant flow along the upslope wall is built. The heat convection contributes immediately, and the Nu departs from the conduction state ($Nu = 1$). For a higher Rayleigh number, $Ra = 2000$, which lies at a supercritical state, Nu for $\gamma = 0°$ is around 1.1. As Ra further increases, e.g. $Ra = 3000$, 4000 or 5000, a noticeable drop on the Nu-curve appears. The change in heat transfer rate

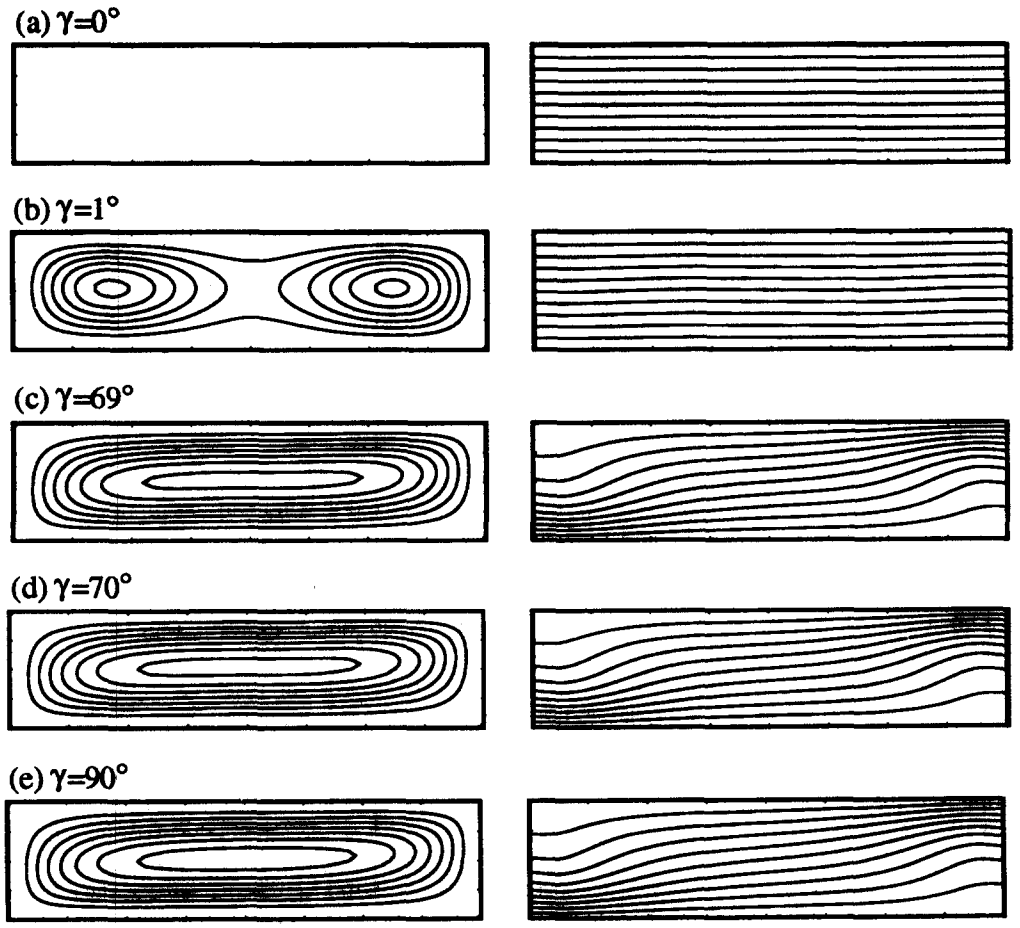

Fig. 4. Streamlines (left column) and isotherms (right column) for $Ra = 1500$ and γ increasing. (a) $\gamma = 0°$, conductive solution; (b) $\gamma = 1°$, the extreme values of ψ are $(\psi_{min}, \psi_{max}) = (0, 0.125)$, and the streamlines drawn are $\psi = 0$ to 0.12 with $\Delta\psi = 0.02$, or in brief, $\psi = 0(0.02)0.12$; (c) $\gamma = 69°$, $(\psi_{min}, \psi_{max}) = (0, 3.624)$ and $\psi = 0(0.5)3.5$; (d) $\gamma = 70°$, $(\psi_{min}, \psi_{max}) = (0, 3.641)$ and $\psi = 0(0.5)3.5$; (e) $\gamma = 90°$, $(\psi_{min}, \psi_{max}) = (0, 3.756)$ and $\psi = 0(0.5)3.5$. In streamline patterns, solid lines: counter-clockwise.

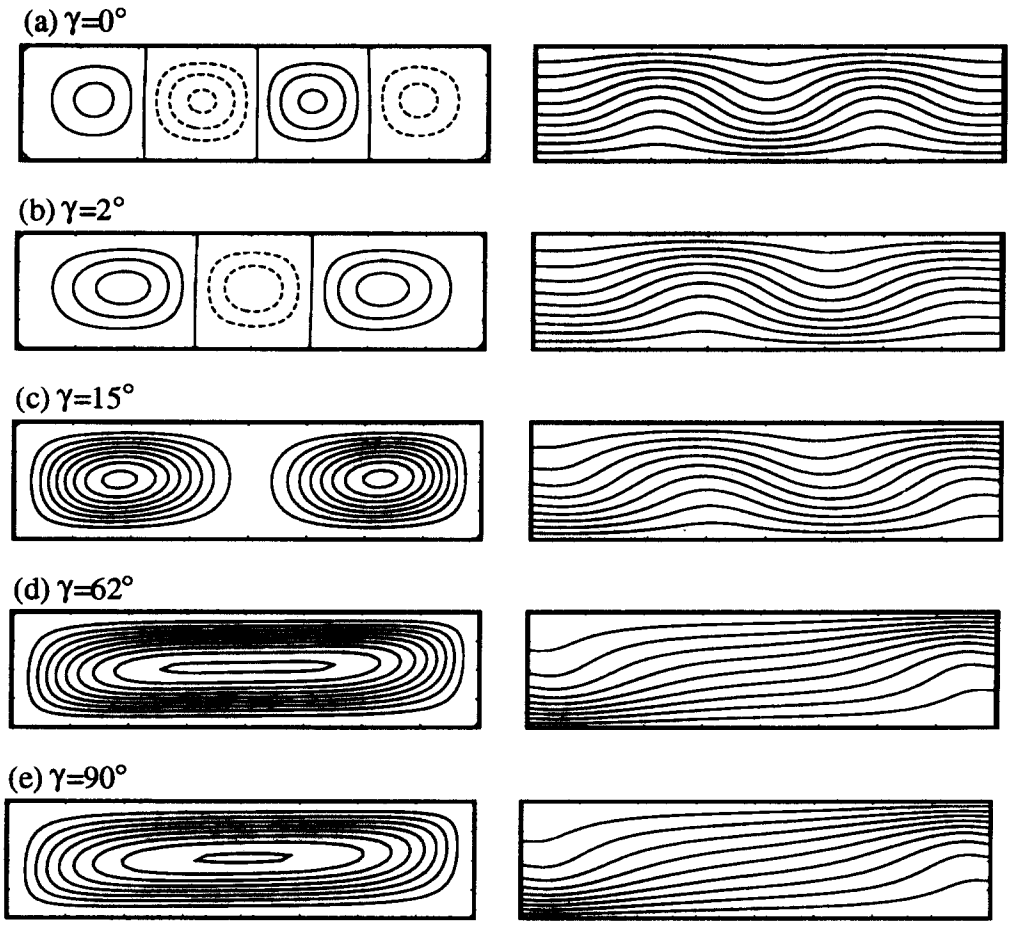

Fig. 5. Streamlines and isotherms for $Ra = 2000$ and γ increasing. (a) $\gamma = 0°$, $(\psi_{min}, \psi_{max}) = (-1.296, 1.296)$ and $\psi = -1.2(0.4)1.2$; (b) $\gamma = 2°$, $(\psi_{min}, \psi_{max}) = (-1.122, 1.413)$ and $\psi = -0.8(0.4)1.2$; (c) $\gamma = 15°$, $(\psi_{min}, \psi_{max}) = (0, 2.498)$ and $\psi = 0(0.3)2.4$; (d) $\gamma = 62°$, $(\psi_{min}, \psi_{max}) = (0, 4.570)$ and $\psi = 0(0.5)4.5$; (e) $\gamma = 90°$, $(\psi_{min}, \psi_{max}) = (0, 4.854)$ and $\psi = 0(0.6)4.8$. In streamline patterns, solid lines: counter-clockwise; dashed lines: clockwise.

implies a transition of the flow pattern. The transition for changing γ can be delayed by increasing Ra. For the cases of $Ra = 10\,000$ and $20\,000$, a relatively small indentation emerges before the occurrence of the catastrophe. It is believed that another mode transition occurs there.

In Fig. 3, the maximum velocities u_{max} and v_{max} in the flow fields corresponding to the cases in Fig. 2 are plotted. Inclination results upslope (downslope) flow along the hot (cold) isothermal walls; therefore, u_{max} increases with γ as shown in Fig. 3(a). It is most interesting that the values of v_{max} in Fig. 3(b) are of the similar trend as the mean Nusselt numbers shown in Fig. 2. Physically, heat is supplied by the hot wall and, except the conduction, it is convected towards the cold wall by the transverse movement of the fluid particles. The larger the transverse velocity, v, the higher the heat transfer rate, Nu. Figure 3(b) demonstrates this close relevance of the transverse velocity v to the heat transfer mechanism. In addition, clearer information about the flow-mode transition can be obtained from the observations on the v_{max} curves.

Flow-mode transition for γ increasing

The streamlines and isotherms at $Ra = 1500$, 2000, 5000 and 20 000 are shown in Figs. 4–7, respectively. In Fig. 4 for $Ra = 1500$, the calculated values of u and v are of the order of 10^{-11}–10^{-10}. According to our experience in the computation, the orders of u and v drop continuously although the decaying rate is slow. The fluid in this subcritical ($Ra < Ra_c$) state is still regarded as stationary. As the enclosure is inclined, $\gamma = 1°$, the shear flow along the two longitudinal walls results a large circulation in which there are two weak sub-cells rotating in the same sense as the primary cell. This two-in-one cellular structure disappears at an inclination angle between 69° and 70° due to stronger upslope/downslope flows along the x-direction. For $\gamma \geqslant 70°$, the flow field is of unicell mode. The isotherms in Fig. 4(b) illustrate a gradual change from a

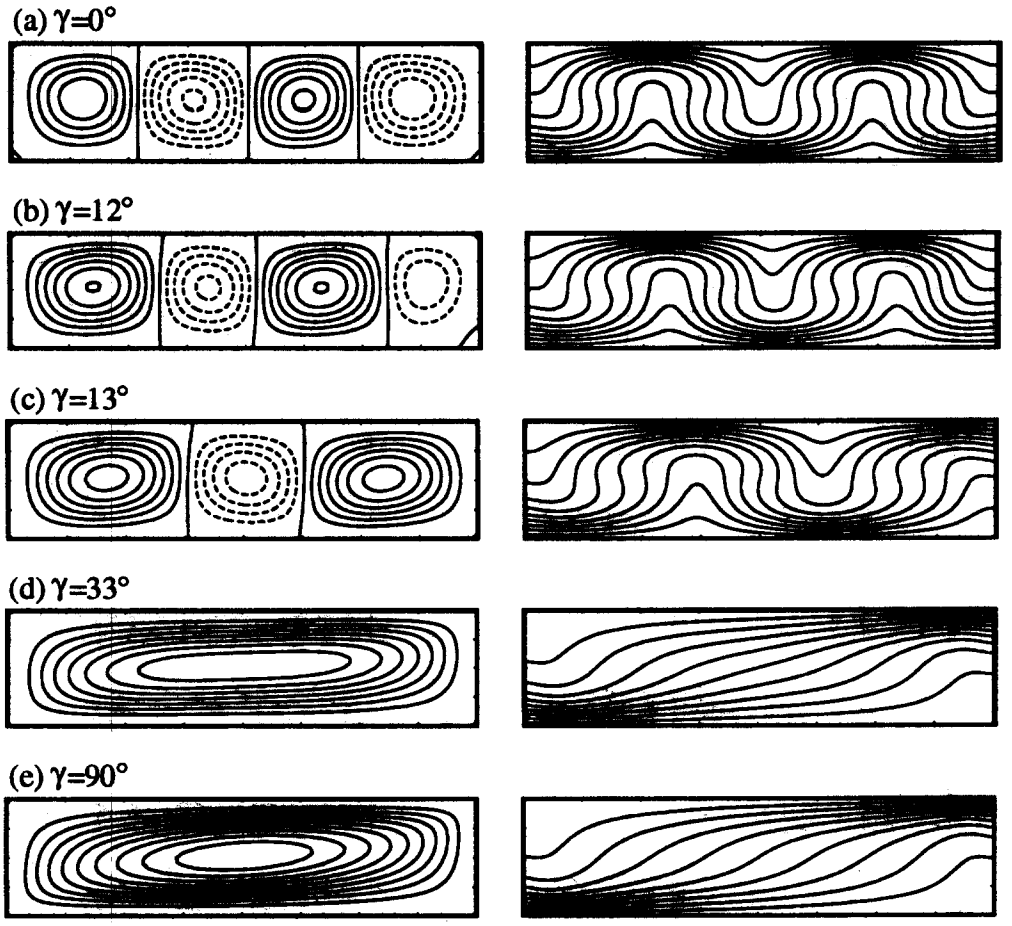

Fig. 6. Streamlines and isotherms for $Ra = 5000$ and γ increasing. (a) $\gamma = 0°$, $(\psi_{min}, \psi_{max}) = (-5.253, 5.253)$ and $\psi = -5.0(1.0)5.0$; (b) $\gamma = 12°$, $(\psi_{min}, \psi_{max}) = (-4.324, 6.081)$ and $\psi = -4.0(1.0)6.0$; (c) $\gamma = 13°$, $(\psi_{min}, \psi_{max}) = (-4.668, 6.487)$ and $\psi = -4.0(1.0)6.0$; (d) $\gamma = 33°$, $(\psi_{min}, \psi_{max}) = (0, 7.783)$ and $\psi = 0(1.0)7.0$; (e) $\gamma = 90°$, $(\psi_{min}, \psi_{max}) = (0, 9.903)$ and $\psi = 0(1.0)9.0$.

stratification state to a skew-symmetric distortion due to the cellular motion. Figure 5 shows the case of $Ra = 2000$, in which the flow appears as a four-cell structure at $\gamma = 0°$. In this slightly super-critical flow, the cellular motion is weak, the right-most cell at the upper end of the inclination enclosure can not resist the upward flow coming from the hot wall and, then, it is smeared out at the inclination angle even as low as $\gamma = 2°$. Hereinafter, the flow structure turns to the three-cell one and the isotherms show the attendant change in temperature field. As the inclination angle increases, the flow pattern changes to a two-in-one cell mode at γ between 14° and 15°, and the latter structure persists until $\gamma = 61°$. At $\gamma = 62°$, the flow field turns to one of unicell mode. For a higher Rayleigh number, $Ra = 5000$ in Fig. 6, the cellular motion becomes stronger due to larger buoyancy and the four-cell structure can maintain for inclination angle up to $\gamma = 12°$. The flow pattern turns to a three-cell structure at $\gamma = 13°$ and retains the same pattern up to $\gamma = 31°$. Subsequently, the unicell mode prevails in the range of $33° \leqslant \gamma \leqslant 90°$. The two-in-one cellular structure appears only in a small region of $31° < \gamma < 33°$. The isotherms change from a highly-distorted state for multi-cell structures at low-γ to a simple pattern for unicell mode at $\gamma \geqslant 33°$. As the Rayleigh number further increases, the occurrence of the mode-transition from four-cell to three-cell can be postponed to a higher value of γ, e.g. $\gamma = 19°$ for $Ra = 20\,000$ in Fig. 7. Also, in the high-Ra case, the complex flow turns to the simple unicell structure at a higher inclination. Similar but highly distorted isotherms as that for $Ra = 5000$ are presented in Fig. 7(b). It is noted that a small corner cell appears in the calculated four-cell structure before the transition to three-cell. The corner cell is essentially a characteristic phenomenon for high Ra (or high driving force).

Hysteresis phenomenon

Due to highly nonlinear nature of the system, dual or multiple solutions may exist. To investigate the hysteresis phenomenon in the problem, the course of

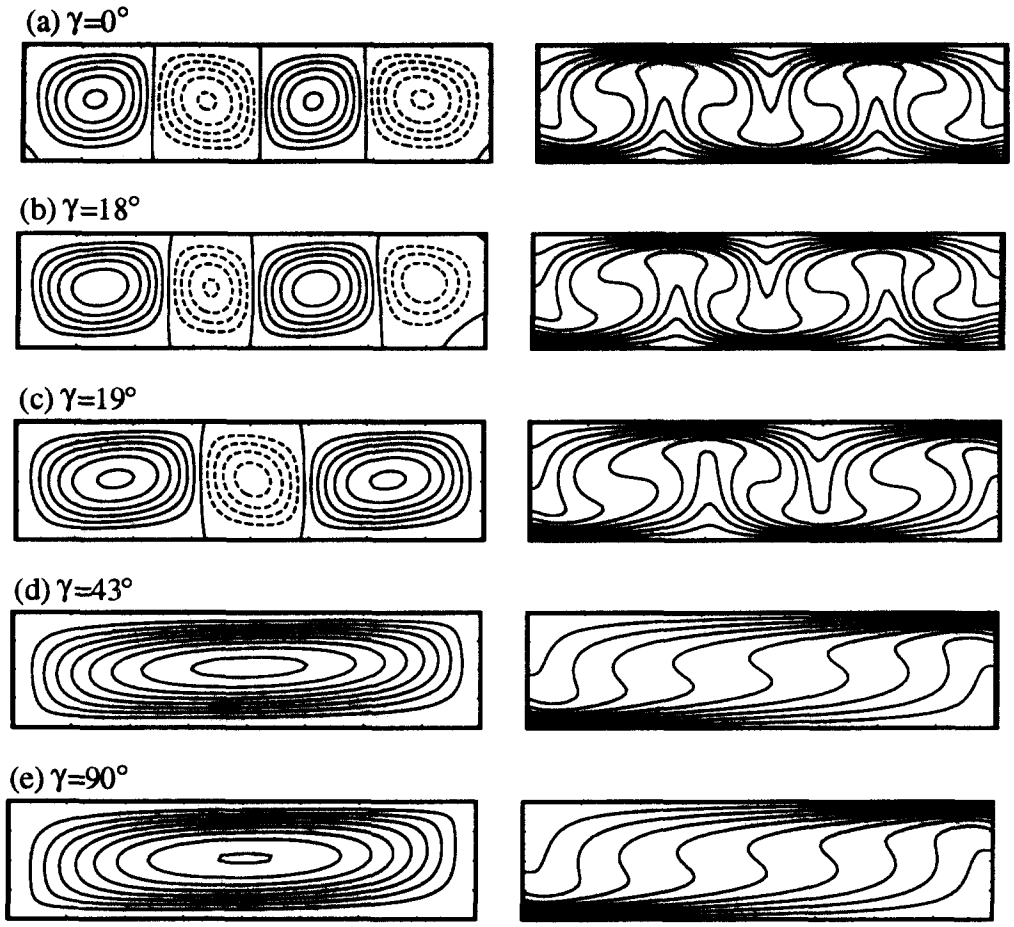

Fig. 7. Streamlines and isotherms for $Ra = 20000$ and γ increasing. (a) $\gamma = 0°$, $(\psi_{min}, \psi_{max}) = (-12.939, 12.939)$ and $\psi = -12.5(2.5)12.5$; (b) $\gamma = 18°$, $(\psi_{min}, \psi_{max}) = (-10.303, 14.443)$ and $\psi = -10(2.5)12.5$; (c) $\gamma = 19°$, $(\psi_{min}, \psi_{max}) = (-11.393, 15.481)$ and $\psi = -10(2.5)15$; (d) $\gamma = 43°$, $(\psi_{min}, \psi_{max}) = (0, 20.890)$ and $\psi = 0(2.5)20.0$; (e) $\gamma = 90°$, $(\psi_{min}, \psi_{max}) = (0, 20.161)$ and $\psi = 0(2.5)20.0$.

the computations are reversed, i.e. low-γ solutions are found by taking the convergent solution at a slightly higher value of γ as the initial guess. It is just equivalent to reducing the inclination in the experiment. Figure 8 shows the comparisons of the calculated mean Nusselt numbers for increasing and decreasing γ. At $Ra < 2000$, no significant difference between the results obtained in the two courses of changing γ. At $Ra = 2000$ in Fig. 8(a), two solutions deviate in a small region of inclination and at $Ra = 3000$ it is more noticeable in the range of $\gamma < 10°$. For $Ra = 4000$ and 5000, an additional hysteresis region near $\gamma = 30°$ emerges and the two dual-solution regions enlarge with increasing Ra. As Ra further increases to $Ra = 10000$ and 20000, the hysteresis prevails in a considerable range of lower inclination. The bifurcation point moves toward high γ as Ra increases. It implies the complexities of the flow field at high heating rates. As an illustrative example of the hysteresis phenomena, the mode transition of the flow and temperature fields at $Ra = 5000$ and with γ-decreasing are shown in Fig. 9 and compared with those for γ increasing in Fig. 6. Comparison shows that the flow-mode transition can be significantly influenced by the course of changing inclination γ.

Parameter maps

Parameter maps are very useful in summarizing the flow patterns for various combinations of the parameters involved. In a small As enclosure the flow structure is simpler, e.g. unicell pattern prevails in steady flow regime for $As = 1$. Although the complexity of the flow structure in large As can be expected, the construction of the parameter maps is very expensive in a computational viewpoint. In the present work, by considering both the interest in the flow complexity and the computational efforts, only the enclosure of $As = 4$ is considered as a typical example to illustrate the diversity of the flow structure and the difference in parameter maps for the γ-increasing and γ-decreasing courses.

Based on the computational results, parameter

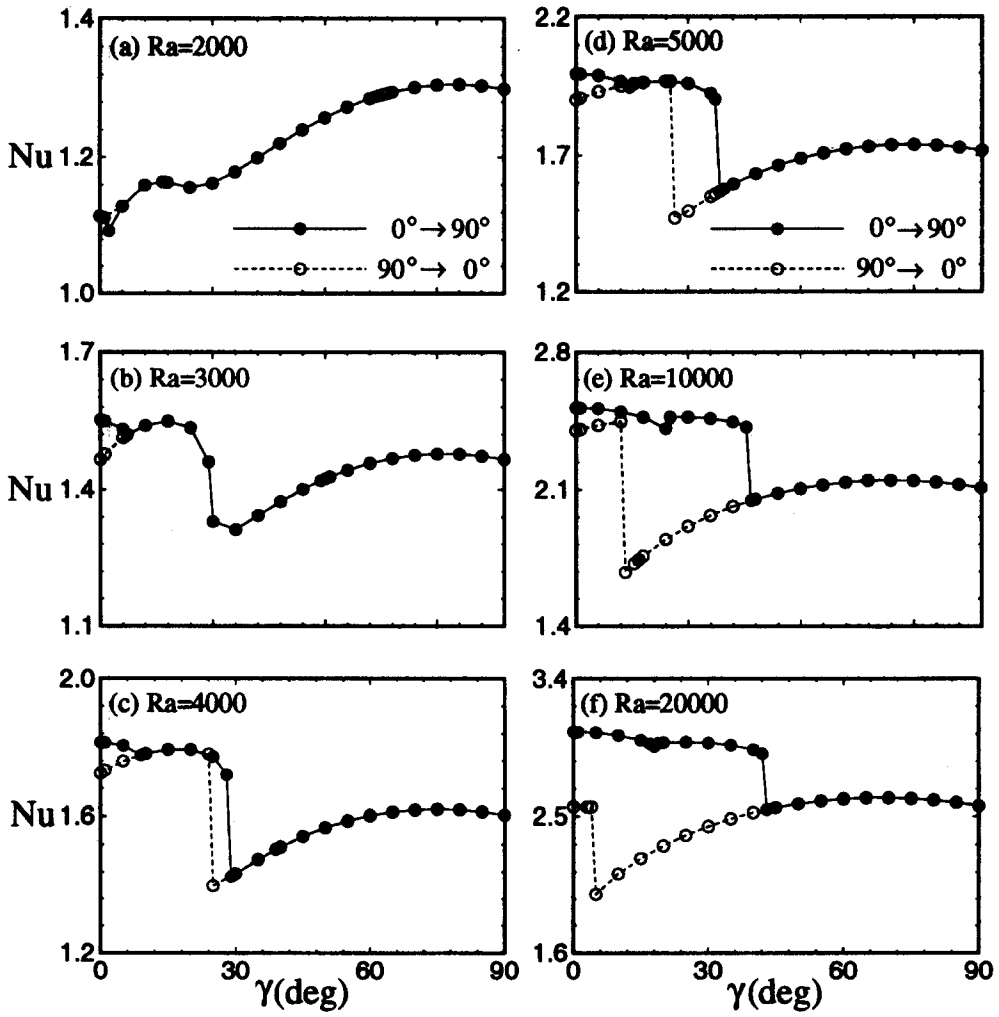

Fig. 8. Hysteresis phenomena denoted by average Nusselt numbers. (a) $Ra = 2000$; (b) $Ra = 3000$; (c) $Ra = 4000$; (d) $Ra = 5000$; (e) $Ra = 10\,000$ and (f) $Ra = 20\,000$.

maps of Ra vs γ for γ-increasing and γ-decreasing, respectively, are constructed as Figs. 10(a) and (b), in which the flow regimes characterized by four-cell, three-cell, two-in-one cell, and unicell are designated. It is revealed that, in Fig. 10(a) for γ-increasing, the multi-cell structures exist in low-γ cases, in which the thermal instability mechanism dominates. With increasing Rayleigh number, the flow regimes of multi-cell structures become large. It is also attributed to the dominant role of the convection cells, while for the high inclination, the unicell mode is prevailing due to the strong upslope flow along the hotter isothermal wall caused by large buoyancy force component in that direction. The strong longitudinal flow destroys the multi-cell (four- and three-cell) structures.

In Fig. 10(b) for the case of decreasing γ, the flow-mode transition is distinct from that for increasing γ. Since the flow fields at large inclination angles are of simpler structure of unicell, the flow tends to maintain the unicell structure as γ decreases from 90°. Therefore, a larger unicell region is shown in the parameter map. Similarly, the simple structure of two-in-one cell can exist at the lower γ, especially in the cases of high Ra. Relatively, the complex flows of the three-cell structure are restricted in a smaller regime, and the four-cell mode even disappears in this γ decreasing course. For Ra lies up to the value of 20 000, three-cell vanishes and two-cell structure emerges at low inclination angles, i.e. $\gamma \leqslant 4°$.

Effects of initial conditions

Effects of the initial condition in inclined cases are reflected in the hysteresis phenomena and dual solutions in some γ-ranges described in the last sections. For the horizontal enclosures, the solution sensitivity to the initial condition of the temperature field is examined by using an enclosure of $As = 3$. Three initial conditions, $\theta_i = 0$, 0.5 and 1.0, are considered. These three values, respectively, correspond to the fluid being initially at the cold-wall temperature, T_c,

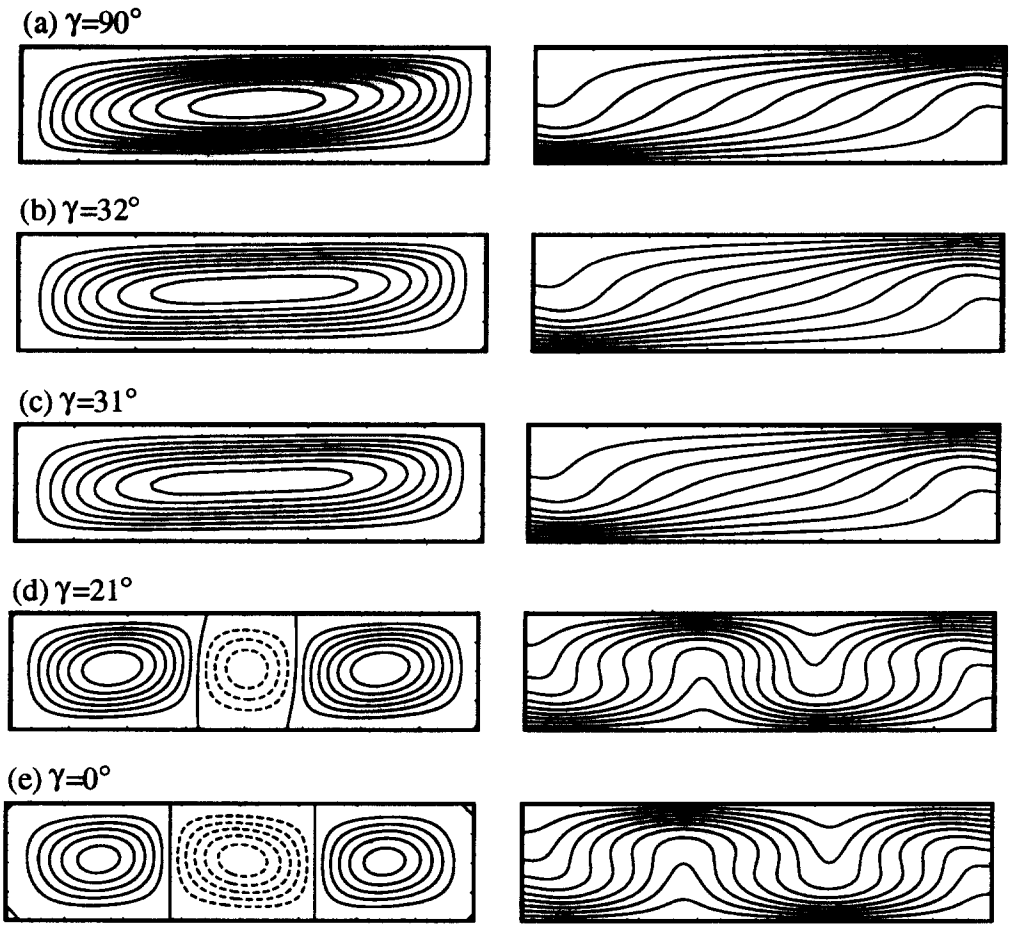

Fig. 9. Streamlines and isotherms for $Ra = 5000$ and γ decreasing. (a) $\gamma = 90°$, $(\psi_{min}, \psi_{max}) = (0, 9.903)$ and $\psi = 0(1.0)9.0$; (b) $\gamma = 32°$, $(\psi_{min}, \psi_{max}) = (0, 7.646)$ and $\psi = 0(1.0)7.0$; (c) $\gamma = 31°$, $(\psi_{min}, \psi_{max}) = (0, 7.505)$ and $\psi = 0(1.0)7.0$; (d) $\gamma = 21°$, $(\psi_{min}, \psi_{max}) = (-3.789, 6.925)$ and $\psi = -3.0(1.0)6.0$; (e) $\gamma = 0°$, $(\psi_{min}, \psi_{max}) = (-5.745, 5.538)$ and $\psi = -5.0(1.0)5.0$.

the average of the cold- and hot-wall temperatures, $(T_c + T_h)/2$ and the hot-wall temperature, T_h. For $\theta_i = 0$, the fluid near the hot bottom wall is heated and tends to rise up. Since the fluids adjacent to the side walls are retarded by the strong viscous effect, the ascending motion is relatively stronger in the central region (x near 1.5). Finally, as shown in Fig. 11(a), a pair of counter-rotating cells with the central fluid arising is formed, while in the cases of $\theta_i = 1$, the situation is reversed. The fluid lies initially at the same temperature as the hot-wall and is suddenly cooled by the top cold wall. The cooled fluid near the top wall tends to descend and, for relatively weaker viscous effect, the fluid in central region moves downward. The resultant vortex-pair rotates in opposed sense as that in the case of $\theta_i = 0$, see Fig. 11(c). In case of $\theta_i = 0.5$, which is an equilibrium state in a conductive sense for the fluid at $y = 0.5$. The fluid at the center of the enclosure, i.e. $(x, y) = (1.5, 0.5)$, tends to remain stationary and becomes a vortex center for the symmetric nature of the thermal state. In this situation, a flow pattern of odd number of cells, e.g. three cells in Fig. 11(b), is more likely constructed.

For odd number of cells in horizontal enclosures with perfect boundary conditions, there are two possible flow patterns, e.g. the three-cell structures of $(+, -, +)$ and $(-, +, -)$. The resultant flow pattern in this case is strongly influenced by the disturbances, either numerical (in computations) or physical (in experiments), emerging in the flow field. Therefore the round-off error distribution in the field, which depends on the numerical scheme (no matter how stable) and the calculation procedure (e.g. direction of line-by-line sweep) used in the computations, may result a preferred one of the two possible flow patterns. However, it is noteworthy that these two flows, $(+, -, +)$ or $(-, +, -)$, are of the same values of the mean Nusselt number in the horizontal enclosures.

Effects of imperfect thermal boundary conditions

Figure 12(a) shows the γ-dependence of the heat transfer rates for the cases of $Ra = 3800$ and $Pr = 5580$ in a square enclosure. The present predictions are compared with the measured data (solid diamond) and the numerical results (solid line) both by Ozoe *et al.* [8]. It is noted that, in Fig. 12(a), as the

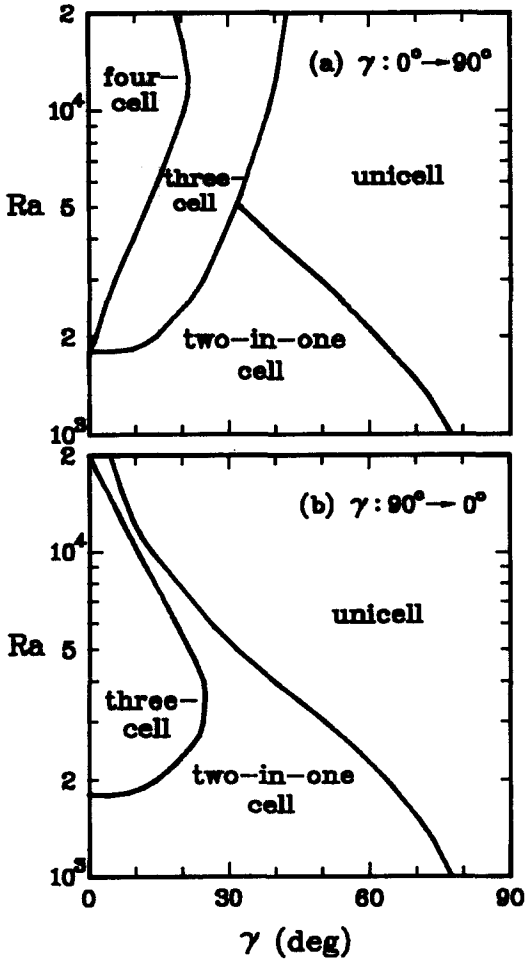

Fig. 10. Parameter maps for natural convection in two-dimensional inclined enclosure. (a) γ-increasing; (b) γ-decreasing.

inclination increases from $\gamma = 0°$, the measured Nu first drops and then turns to rise at about $\gamma = 5°$. This trend was missed in the two-dimensional numerical predictions of Ozoe *et al.* in which Nu is monotonic in the low-γ regime. For a higher Rayleigh number, in Fig. 12(b), the same behavior is displayed. In a later report by Ozoe *et al.* [13] they claimed that it is attributed to the three-dimensional effect. Herein, another effect arising from the imperfection of the thermal boundary conditions is investigated.

In the present study, the mismatch is presumed to be caused by the imperfection of the thermal boundary conditions in the experiments. To demonstrate this theory, wall temperature on the upper boundary, $\theta(x, 1) = 0$, is replaced by $\theta(x, 1) = \varepsilon(1 - 2x/As)$, where ε denotes a perturbation parameter for the imperfection of wall-temperature uniformity. The case of $\varepsilon = 0$ corresponds to that of perfect isothermal-wall condition. By considering $\varepsilon = 0.0005$, which results a non-uniformity of $\pm 0.05\%$ in the upper wall temperature, the predicted values of Nu, denoted by the solid triangles in Fig. 12(a), for $\gamma \leqslant 5°$ behave totally different from the corresponding cases of $\varepsilon = 0$ or perfect condition. However, the solutions return back to the curve for $\varepsilon = 0$ at $\gamma = 6°$. The predicted change-over occurs at the inclination between 5 and 6°, which agrees well with the experimental data although the peak values are rather different. The computed Nu-peak is sharper than the measured data. It is believed that the sharpness stems from the two-dimensionality of the computational model. Another value, $\varepsilon = 0.005$, is also used in the computation. There is no significant difference between the Nusselt numbers for $\varepsilon = 0.005$ and $\varepsilon = 0.0005$. It implies that the small disturbances result in insignificant change in physical quantity such as heat transfer rate as long as $\varepsilon \neq 0$. But even a very small ε, e.g. $\varepsilon = 0.0005$, can produce remarkable deviation from the case of $\varepsilon = 0$. Obviously, the imperfection of the thermal boundary condition plays essentially a triggering role for a mode-transition.

For the case of $Ra = 4950$ and $Pr = 5220$ shown in Fig. 12(b), Ozoe *et al.* measured heat transfer rates with γ-increasing (solid rhombuses) as well as γ-decreasing (open rhombuses). In the γ-increasing course, the present prediction with the disturbed thermal boundary condition ($\varepsilon = 0.0005$), can also catch the bifurcation trend although the predicted change-over angle slightly deviates from the experimental result. For γ-decreasing, the present results with either the perfect and disturbed conditions are close to the predictions of Ozoe *et al.* [8].

To manifest the triggering role of the imperfection of the wall condition, the streamlines and isotherms for the horizontal enclosure with $\varepsilon = 0$, -0.0005 and 0.0005 are shown in Figs. 13(a), (b) and (c), respectively. In the perfect case of $\varepsilon = 0$, the cell rotates in counter-clockwise sense. In the case of $\varepsilon = -0.0005$ in Fig. 13(b), the right-half of the cold-wall lies at a slightly higher temperature than the left-half, which also results in a cellular motion of the counter-clockwise rotation as that for $\varepsilon = 0$. However, the imperfection of the wall temperature with $\varepsilon = 0.0005$ alters the rotating sense of the cell due to different perturbation in cold-wall temperature. For $\varepsilon = 0$ and -0.0005, the inclination of the enclosure can enhance the counter-clockwise rotation as well as the heat transfer rates. For the inclined case of $\varepsilon = 0.0005$, however, the upslope shear flow due to buoyancy produces a counter effect on the clockwise rotation of the cell, and the heat transfer performance degraded. At $\gamma = 6°$, the effect is large enough to reverse the rotational sense of the cellular motion, the flow pattern bifurcates and turns back to the upper branch of the solutions, see Fig. 14.

CONCLUDING REMARKS

A numerical investigation for a two-dimensional differentially heated enclosure has been performed. Based on the computational results, the following

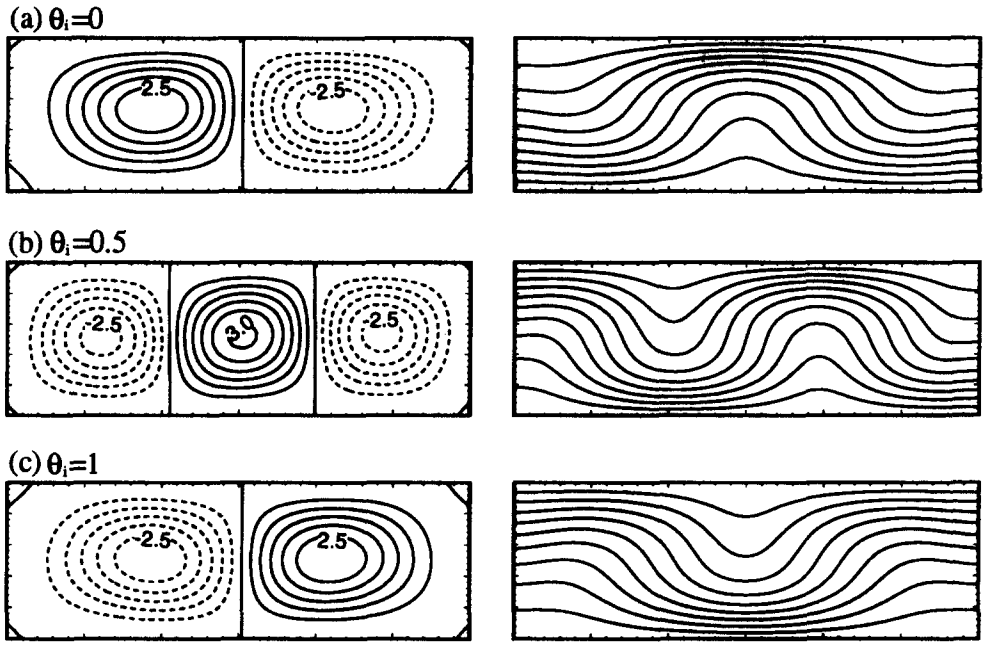

Fig. 11. Effects of initial temperature field on flow pattern for $Ra = 3000$ and $Pr = 0.71$ in a horizontal enclosure of $As = 3$. (a) $\theta_i = 0$, $(\psi_{min}, \psi_{max}) = (-3.007, 3.007)$ and $\psi = -2.5(0.5)2.5$; (b) $\theta_i = 0.5$, $(\psi_{min}, \psi_{max}) = (-2.786, 3.142)$ and $\psi = -2.5(0.5)3.0$; (c) $\theta_i = 1.0$, $(\psi_{min}, \psi_{max}) = (-3.007, 3.007)$ and $\psi = -2.5(0.5)2.5$. In streamline patterns, solid lines: counter-clockwise; dashed lines: clockwise.

conclusions can be drawn:

(1) The enhancement of heat transfer rates in the cases of high Ra and γ is closely related to the mechanism of variation in transverse velocity (v). In the flow with a larger transverse velocity, the natural convection heat transfer is strong.

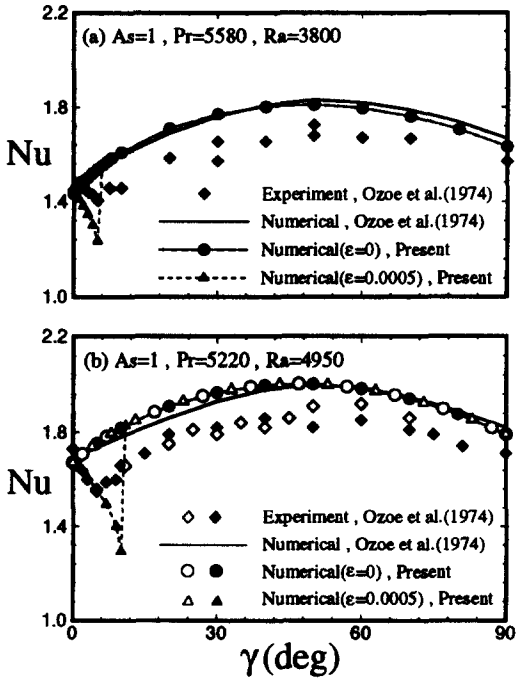

Fig. 12. Comparisons of the present predictions and the measured data for natural convection in a square enclosure at (a) $Ra = 3800$ and $Pr = 5580$; (b) $Ra = 4950$ and $Pr = 5220$. The solid and open notations are results for γ-increasing and γ-decreasing, respectively.

(2) The possible flow modes (or flow patterns) in the enclosure of $As = 4$ are four-cell, three-cell, two-in-one cell and unicell. For a fixed value of Ra, the transition of the flow mode strongly depends on the competition of the buoyant flow and the shear flow (along the heating and cooling walls) due to inclination. For γ increasing, the multi-cell structures can exist at low inclination angles. The flow regimes of multi-cell structures in the map extend with increasing Ra. Whereas the unicell mode prevails in high inclination since the strong longitudinal (x-direction) flow destroys the multi-cell (four- and three-cell) structures.

(3) For $As = 4$ in the present work, hysteresis phenomenon appears for $Ra \geqslant 2000$. In the course of γ decreasing from 90° to 0°, the flow map is different from that for γ increasing. The computational results in the course of γ-decreasing reveal that the simple flow patterns of unicell and two-in-one cell prevail in most parts of the map. The more complex flow of three-cell is restricted in a small region of low-γ. Furthermore, the four-cell structure disappears.

(4) Flow pattern formation is very sensitive to the initial state of the flow field. In inclined enclosures, the effects are reflected on the hysteresis phenomena and dual solutions in some regions of inclination angle. For horizontal cases, the resultant flow pattern may also strongly depend on the initial condition of fluid temperature. Similarly, to generate a flow pattern

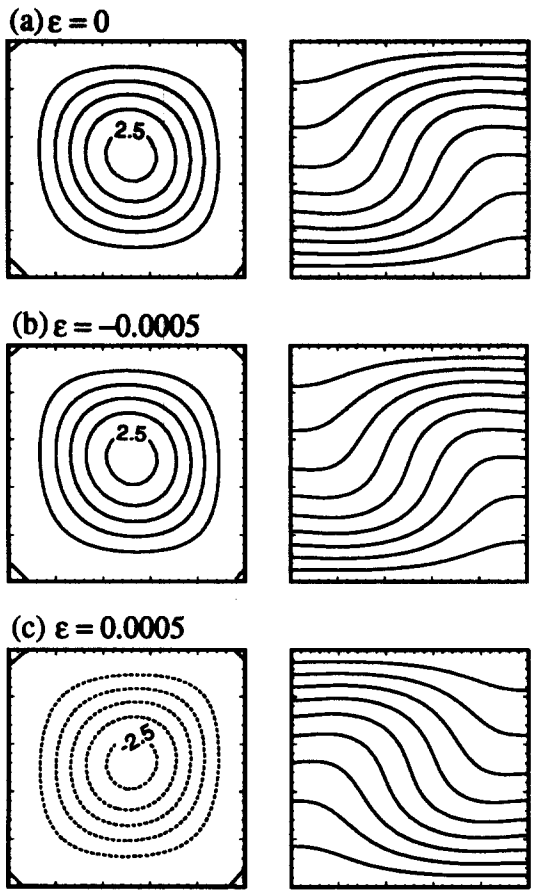

Fig. 13. Streamlines and isotherms for $As = 1$, $Ra = 3800$, $Pr = 5580$ and $\gamma = 0°$. (a) $\varepsilon = 0$, $(\psi_{min}, \psi_{max}) = (0, 2.734)$ and $\psi = 0(0.5)2.5$; (b) $\varepsilon = -0.0005$, $(\psi_{min}, \psi_{max}) = (0, 2.736)$ and $\psi = 0(0.5)2.5$; (c) $\varepsilon = 0.0005$, $(\psi_{min}, \psi_{max}) = (-2.736, 0)$ and $\psi = -2.5(0.5)0$.

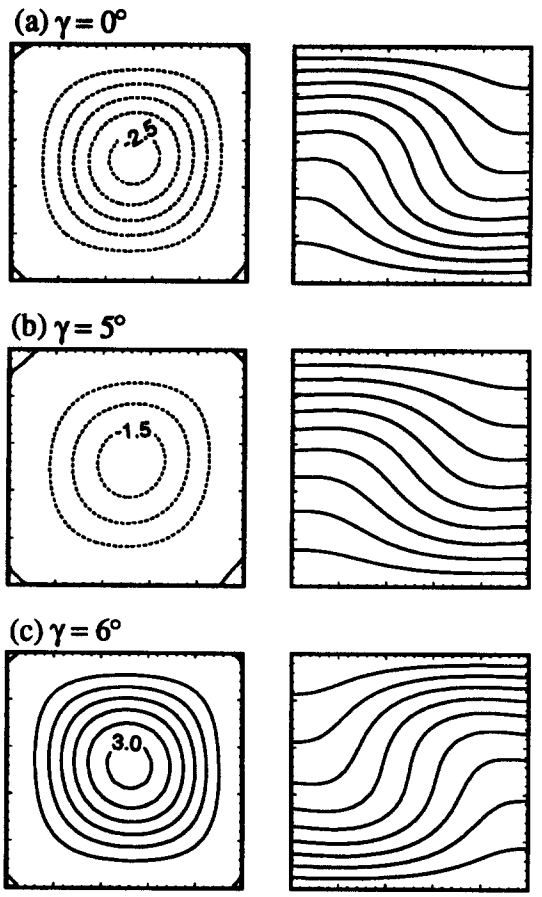

Fig. 14. Change-over process for $As = 1$, $Ra = 3800$, $Pr = 5580$, $\varepsilon = 0.0005$ and (a) $\gamma = 0°$, $(\psi_{min}, \psi_{max}) = (-2.736, 0)$ and $\psi = -2.5(0.5)0$; (b) $\gamma = 5°$, $(\psi_{min}, \psi_{max}) = (-1.794, 0)$ and $\psi = 0(0.5)1.5$ and (c) $\gamma = 6°$, $(\psi_{min}, \psi_{max}) = (0, 3.216)$ and $\psi = 0(0.5)3.0$.

under a specific condition in laboratory, initial state setting is critical to the resultant flow structure.

(5) Non-uniformity of the wall temperature may result in a different flow mode from that of perfection conditions. The present numerical study has demonstrated that the imperfection of the thermal boundary condition can be a trigger for the mode-transition. Furthermore, in addition to the three-dimensionality, the imperfection in thermal boundary condition, which is quite common in experiments, is one of the possible causes for the mismatch of the numerical prediction and the measured data.

REFERENCES

1. K. T. Yang, Transitions and bifurcations in laminar buoyant flows in confined enclosures, *ASME J. Heat Transfer* **110,** 1191–1203 (1988).
2. D. Dropkin and E. Somerscales, Heat transfer by natural convection in liquids confined by two parallel plates which are inclined at various angles with respect to the horizontal, *ASME J. Heat Transfer* **87,** 77–84 (1965).
3. J. E. Hart, Stability of the flow in a differentially heated inclined box, *J. Fluid Mech.* **47,** 547–576 (1971).
4. K. G. T. Hollands and L. Konicek, Experimental study of the stability of differentially heated inclined air layers, *Int. J. Heat Mass Transfer* **16,** 1467–1476 (1973).
5. J. N. Arnold, I. Catton and D. K. Edwards, Experimental investigation of natural convection in inclined rectangular regions of differing aspect ratios, *ASME J. Heat Transfer* **98,** 67–71 (1976).
6. I. Catton, P. Ayyaswamy and R. M. Clever, Natural convection flow in a finite, rectangular slot arbitrarily oriented with respect to the gravity vector, *Int. J. Heat Mass Transfer* **17,** 173–184 (1974).
7. M. Strada and J. C. Heinrich, Heat transfer rates in natural convection at high Rayleigh numbers in rectangular enclosures: a numerical study, *Numer. Heat Transfer* **5,** 81–93 (1983).
8. H. Ozoe, H. Sayama and S. W. Churchill, Natural convection in an inclined square channel, *Int. J. Heat Mass Transfer* **17,** 401–406 (1974).
9. H. Ozoe, H. Sayama and S. W. Churchill, Natural convection in an inclined rectangular channel at various aspect ratios and angles—experimental measurements, *Int. J. Heat Mass Transfer* **18,** 1425–1431 (1975).
10. H. Ozoe, H. Sayama and S. W. Churchill, Natural convection in a long inclined rectangular box heated from below—I. Three-dimensional photography, *Int. J. Heat Mass Transfer* **20,** 123–129 (1977).
11. H. Ozoe, K. Yamamoto, H. Sayama and S. W.

Churchill, Natural convection in a long inclined rectangular box heated from below—II. Three-dimensional numerical results, *Int. J. Heat Mass Transfer* **20,** 131–139 (1977).
12. H. Ozoe, N. Sato and S. W. Churchill, Experimental confirmation of the three-dimensional helical streaklines previously computed for natural convection in inclined rectangular enclosures, *Int. Chem. Engng* **19,** 454–462 (1979).
13. H. Ozoe, K. Yamamoto and S. W. Churchill, Three-dimensional numerical analysis of natural convection in an inclined channel with a square cross section, *A.I.Ch.E. J.* **25,** 709–716 (1979).
14. H. Ozoe, K. Fujii, N. Lior and S. W. Churchill, Long rolls generated by natural convection in an inclined, rectangular enclosure, *Int. J. Heat Mass Transfer* **26**(10), 1427–1438 (1983).
15. K. Okada and H. Ozoe, Various computational conditions of oscillatory natural convection of zero Prandtl number fluid in an open boat heated and cooled from opposing vertical walls, *Numer. Heat Transfer A* **23,** 171–187 (1993).
16. E. M. Sparrow, R. J. Goldstein and V. K. Jonsson, Thermal instability in a horizontal fluid layer: effect of boundary conditions and non-linear temperature profile, *J. Fluid Mech.* **18,** 513–528 (1964).
17. R. Kessler, Nonlinear transition in three-dimensional convection, *J. Fluid Mech.* **174,** 357–379 (1987).
18. C. Gau and D. J. Jeng, Solutal convection and mass transfer in inclined enclosures, *AIAA J. Thermophys. Heat Transfer* **9**(2), 262–269 (1995).
19. G. de Vahl Davis and I. P. Jones, Natural convection in a square cavity: a comparison exercise, *Int. J. Numer. Meth. Fluids* **3,** 227–248 (1983).
20. J. P. Van Doormaal and G. D. Raithby, Enhancements of SIMPLE method for predicting incompressible fluid flows, *Numer. Heat Transfer* **7,** 147–163 (1984).